Lab on a Chip

PAPER

View Article Online
View Journal | View Issue

Cite this: *Lab Chip*, 2019, **19**, 2114

Spatial presentation of biological molecules to cells by localized diffusive transfer†

Mary C. Regier, [abcd] Emily Olszewski,[ab] Christoph C. Carter,[e] John D. Aitchison, [ef] Alexis Kaushansky, [eg] Jennifer Davis,[abh] Erwin Berthier,[i] David J. Beebe[cd] and Kelly R. Stevens *[abh]

Cellular decisions in human development, homeostasis, regeneration, and disease are coordinated in large part by signals that are spatially localized in tissues. These signals are often soluble, such that biomolecules produced by one cell diffuse to receiving cells. To recapitulate soluble factor patterning *in vitro*, several microscale strategies have been developed. However, these techniques often introduce new variables into cell culture experiments (*e.g.*, fluid flow) or are limited in their ability to pattern diverse solutes in a user-defined manner. To address these challenges, we developed an adaptable method that facilitates spatial presentation of biomolecules across cells in traditional open cultures *in vitro*. This technique employs device inserts that are placed in standard culture wells, which support localized diffusive pattern transmission through microscale spaces between device features and adherent cells. Devices can be removed and cultures can be returned to standard media following patterning. We use this method to spatially control cell labeling with pattern features ranging in scale from several hundred microns to millimeters and with sequential application of multiple patterns. To better understand the method we investigate relationships between pattern fidelity, device geometry, and consumption and diffusion kinetics using finite element modeling. We then apply the method to spatially defining reporter cell heterogeneity by patterning a small molecule modulator of genetic recombination with the requisite sustained exposure. Finally, we demonstrate use of this method for patterning larger and more slowly diffusing particles by creating focal sites of gene delivery and infection with adenoviral, lentiviral, and Zika virus particles. Thus, our method leverages devices that interface with standard culture vessels to pattern diverse diffusible factors, geometries, exposure dynamics, and recipient cell types, making it well poised for adoption by researchers across various fields of biological research.

Received 4th February 2019,
Accepted 9th May 2019

DOI: 10.1039/c9lc00122k

rsc.li/loc

Introduction

In multicellular organisms, individual cells maintain life by making complex and coordinated decisions within larger populations of cells.[1] Many of these decisions are based on soluble signals that are localized spatially.[2] For example, spatially and temporally patterned cues (*e.g.*, growth factors, metabolites, and damage associated signals) orchestrate phenotype and subtype heterogeneity to build, maintain, and rebuild tissues during development, homeostasis, and regeneration.[2–6] And during pathogenesis and infection, cells respond to localized insults that often spread across the tissue.[7,8] Despite the known role of multiscale positional cues in organisms, most *in vitro* experiments to measure, model, and manipulate cellular processes are still performed by dosing soluble biological molecules (*i.e.*, biomolecules) homogenously into cell cultures. The ability to spatially deposit soluble biomolecules throughout the course of a cell culture experiment would enable scientists to mechanistically probe how complex positional cues direct biological events.

Spatial positioning of soluble biomolecules in macroscale, "open" culture dishes and well plate formats most commonly used by biologists has been prevented by convective mixing

[a] *Department of Bioengineering, University of Washington, 98195 Seattle, USA. E-mail: ksteve@uw.edu*
[b] *Institute for Stem Cell and Regenerative Medicine, University of Washington, 98109 Seattle, USA*
[c] *Department of Biomedical Engineering, University of Wisconsin – Madison, 53706 Madison, USA*
[d] *Carbone Cancer Center, University of Wisconsin – Madison, 53792 Madison, USA*
[e] *Seattle Children's Research Institute, 98109 Seattle, USA*
[f] *Institute for Systems Biology, 98109 Seattle, USA*
[g] *Department of Global Health, University of Washington, 98104 Seattle, USA*
[h] *Department of Pathology, University of Washington, 98195 Seattle, USA*
[i] *Department of Chemistry, University of Washington, 98195 Seattle, USA*
† Electronic supplementary information (ESI) available. See DOI: 10.1039/c9lc00122k

that disrupts patterning.[9] To overcome this challenge and facilitate biomolecule patterning, a range of specialized microscale technologies, such as microfluidic gradient generators, have been developed.[10–14] Most microscale devices pattern solutes by leveraging limited fluidic mixing in laminar flow,[15–17] diffusion through porous matrices,[11,18] or pressure driven injection of solutes into culture chambers.[19,20] Solutes have also been patterned using hydrodynamic focusing at the tip of microfluidic probes[21–24] or by creating immiscible media phases that can be dispensed across culture surfaces.[25]

However, the majority of such technologies have not been widely adopted in biological research, possibly because they either rely on specialized equipment such as external pumps,[12,21,23,26] motorized stages or probes,[24,27] or pneumatic fluid handlers[28,29] that are not readily available in biology labs, require modification to cell culture media,[25] culture substrate alterations,[30,31] or dissociation and recovery procedures,[32,33] expose cells to stimuli that induce mechanotransduction, such as fluid shear or direct cell contact,[21,23,34] or are limited in the area that can be stimulated simultaneously as they require rastering of a probe.[21,25] As just a few examples, patterning solutes using immiscible 4% PEG (8 kDa) and 8% dextran (500 kDa) carrier medias[25] also increases media viscosity, thus altering transport of nutrients and media components to cells (since relative diffusivity would range from ~0.9–~0.25 for a 4% volume fraction polymer depending on solute size).[35] Further, even low shear stresses as small as 63μPa and less or alterations in substrate mechanics (~1 kPa or less) can alter cell signaling, phenotype, and morphology, especially if such exposures are sustained.[36–40]

Because of these barriers to biological implementation, others have sought to develop technologies for spatial control that can be inserted into existing cell culture vessels (*i.e.* well plates). Such technologies include commonly used Transwell inserts (or Boyden chambers)[41] as well as custom culture segregating devices.[42] Some inserts have been developed that facilitate spatial patterning of soluble biomolecules, but they have relied on embedded microfluidic networks that are fed by pressure driven flow.[12,43,44] In addition to their dependence on external fluidic pumps, existing platforms have been limited in the type of solutes that can be patterned, in patterned area per well, in achievable pattern dynamics, and/or in feasible pattern geometries. While these technologies are important steps forward, the ability to spatially deliver soluble factors to cells in standard well plates in a user-defined and technically straightforward manner has thus remained elusive.

To address this challenge, we aimed to develop a technique that enables spatially localized transfer of biomolecules to cells in open cultures without the need for fluidics or specialized culture media and substrates. In our method, adaptable cell culture inserts are transiently placed within established culture systems to facilitate the positional transfer of biomolecules to cells. These devices stabilize culture media against convective mixing by locally confining cell media to the microscale physical regime governed by interfacial forces, intermolecular forces, and diffusion-based transport.[45,46] Importantly, the use of a narrow transfer gap between the device and the cells enables passive (flow-free) transfer of a preformed pattern without physically contacting and disrupting the cells.

Additionally, our devices can be used to pattern biomolecules across a range of length scales relevant to human pathology and physiology (<1 mm^2 to ~100 mm^2) simultaneously (without rastering), are compatible with cell culture media as dictated by cell type and experiment, and can be operated with standard laboratory equipment (no fluidic pumps or motorized stages). Here, we use this method to spatially transfer particles ranging in size from small molecules (<1 nm diameter) to viral particles (>100 nm diameter) to cells in well plate cultures. These studies establish a new method capable of spatially regulating cellular labeling, genetic heterogeneity, and viral pathogenesis *in vitro*.

Results and discussion

Solute patterning in cell culture using proximity-aided diffusion

To pattern biomolecules in cell culture, we developed an approach based on simple and adaptable cell culture inserts ("devices"). In this approach, devices contain either patterned topographical features coated with hydrogel (Fig. 1A, left) or distinct hydrogel reservoirs (Fig. 1B, left). Devices are first loaded with spatially-localized biomolecules by absorbing biomolecules onto the topographical features (Fig. 1A) or within reservoirs (Fig. 1B). Devices are then inverted and placed in cell culture wells filled completely with media (with the pattern transfer surface facing down). Media in the well is aspirated to lower the device uniformly until it contacts the bottom of the well *via* offset rings or feet that are located at the outer edges of the device. Due to the fluidic resistance within the hydrogel, the device retains the pattern during device lowering despite fluid flow from below the device. Fine control of the separation distance between device features and cells is achieved by precise micromachining of the device's offset rings or feet. Thus, insertion of loaded devices into a cell culture well enables device features and patterned biomolecules to be placed very near (~100 μm separation) to cell culture substrates (Fig. 1A and B, center).

The narrow separation between device and cells creates regions with high resistance to flow and prevents the formation of convective currents in open cultures. This fluidic stability enables localized and rapid diffusion of biomolecules from the device to the underlying cells (Fig. 1A and B, right). Proximity allows for high fidelity pattern transfer, while importantly also avoiding physical contact with the underlying monolayer. Following biomolecule diffusion to cells (5 min – 24 h), device inserts are removed from cell cultures. For removal, devices are simply floated from the culture surface through the addition of wash media. Importantly, disruption and "smearing" of the pattern with media addition is

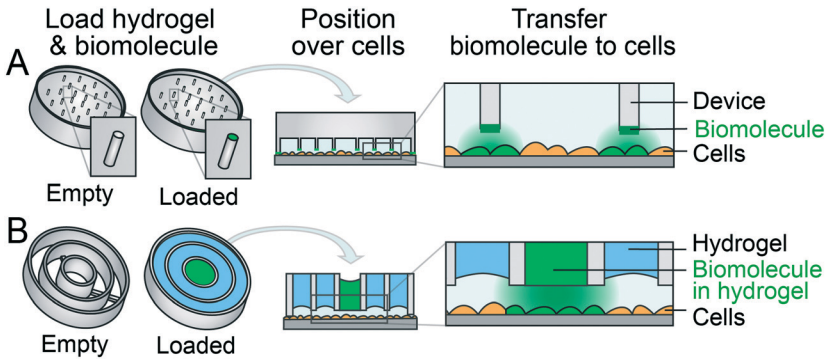

Fig. 1 Approach for proximity-based diffusive transfer of biomolecule patterns. (A) Device inserts with features extending to within 100 μm of the cell culture surface were coated in dilute agarose and biomolecule. Loaded devices were then positioned above cells in a 24-well plate to allow for patterned diffusive transfer of absorbed biomolecules to cells. (B) Alternatively, distinct agarose reservoirs were loaded with biomolecules and then positioned above cells to facilitate patterned diffusive transfer of biomolecule solutes.

counteracted by the vast dilution from $\sim 1 \times 10^2$ to $\sim 1 \times 10^{13}$ final concentration dilution of the solute. Owing to device transience, cells remain accessible and can be manipulated according to standard cell culture procedures.

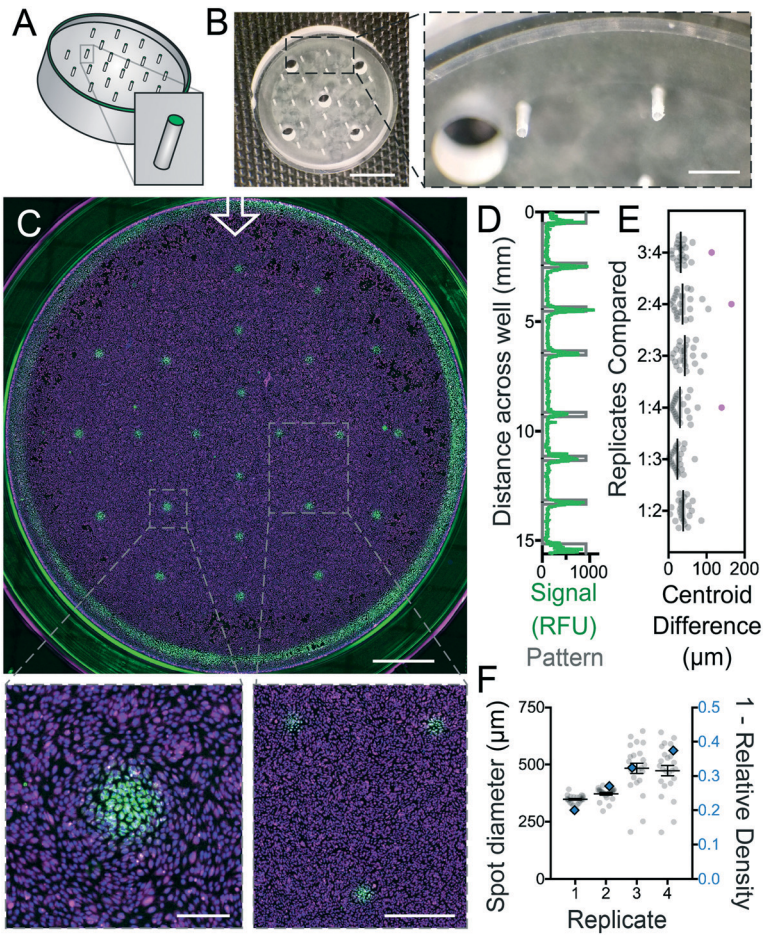

Fig. 2 Precise patterning of small molecule cell tracking dyes. (A) CellTracker dye was adsorbed to (B) micromilled polystyrene pillars coated with agarose and then transferred to cells. (C) After device removal, the pattern of CellTracker dye-labeled cells corresponded with pillar array pattern of the device. Quantification of labeling showed (D) agreement with the designed pattern, (E) precision of spot positioning between replicates (purple spots indicate comparisons between a single spot in replicate 4 that deviated in location from other replicates), and (F) consistent spot size that varied with cell density (blue diamonds). Scale bars: (B left) 5 mm; (B right) 1 mm; (C top) 2 mm; (C bottom left) 250 μm; (C bottom right) 1 mm.

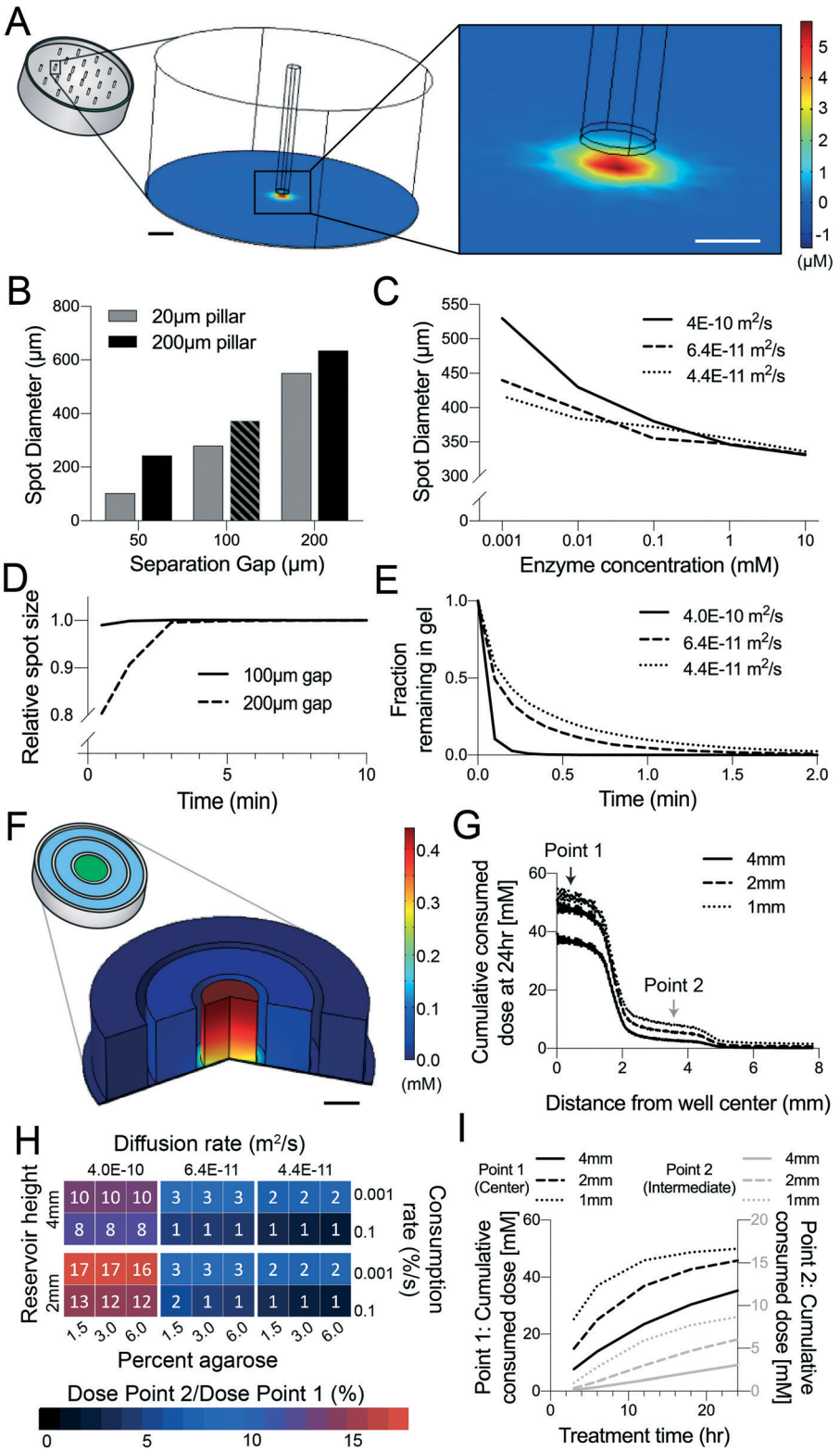

Fig. 3 Finite element modeling of patterning. (A) A single pillar was modeled in Comsol software using diffusion and reaction parameters for CellTracker molecules as well as our experimental device geometry. Patterned spot sizes were quantified for changes in how parameters affect (B) device geometry, (C) molecule diffusion and enzyme kinetics. The dynamics of patterning was quantified for (D) spot size and (E) depletion of the gel at the pillar tip. (F) For sustained patterning larger, concentric reservoirs were modeled. (G) For different reservoir heights and given a cell layer with a 0.1%/s consumption efficiency, cumulative consumption of the patterned small molecule was quantified. The relative concentration at point 2 compared to point 1 as designated in (G) was (H) quantified for different molecule diffusion rates and agarose concentrations (with hinderance coefficients reflecting molecule size and agarose concentration) given a reservoir height of 4 mm or 2 mm and consumption rates of 0.1% or 0.001%. (I) For cumulative consumption was tracked over time for point 1 and point 2 designated in (G). Scale bars: (A) 200 μm, (G) 2 mm.

Rapid bolus delivery for localization of cell labels

We examined the fidelity with which this approach facilitates spatial patterning of solutes by characterizing patterned transfer of small molecules to cells. To do this, we transferred small molecule CellTracker dyes, which become fluorescent and membrane-impermeable upon passive cell entry. Devices with a micromachined array of pillars (Fig. 2A and B) were first dipped into dilute agarose solution and then into a concentrated CellTracker solution. Loaded devices were then transiently inverted over human umbilical vein endothelial cells (HUVECs) in 24-well plate wells to facilitate diffusive transfer. Upon device removal (5 min after insertion), we observed a 1:1 pattern of fluorescent cell clusters that corresponded with pillar array geometry (Fig. 2C and D). When comparing replicate in-cell patterns we noted that 91 of 92 spots were positioned as expected, with centroids within 100 μm of corresponding spot centroids in replicate cultures (58.0 ± 3.5 μm, Fig. 2E). We also observed evidence of limited lateral diffusion as 420 ± 10 μm diameter spots were patterned from 200 μm pillars (Fig. 2F). Spot size was linearly related to the cell-free area (1 − density) with R^2 = 0.69, indicating that patterning precision increases with increasing density, likely through local uptake by cells that limits lateral diffusion. These data demonstrate the ability to spatially localize small molecule cell tracking labels to cells with high resolution by inserting a passive patterning device into standardized cell culture wells. This approach to pattern cell labeling could be used to spatially register ("zipcode") cells for live cell tracking, or prior to culture dissociation and downstream analyses (*e.g.*, single cell RNA sequencing) to address the loss of positional information in such studies.[47–49]

Modeling diffusion and reaction contributions to pattern resolution and dynamics

To probe how the resolution of this diffusion-based method would be affected by changes in transport parameters, reaction kinetics, and timing we next used a finite element modeling approach. We focused our modeling on situations that would occur in cultures of living cells. *i.e.*, those in which the solute interacts with or is taken up by the cells. For example, the active form of Tamoxifen, 4-hydroxytamoxifen (referred to simply as Tamoxifen here), binds the estrogen receptor (preventing binding of endogenous estrogen) and the complex is translocated to the nucleus were it and other co-factors influence gene expression.[50] Similarly, CellTracker signal requires diffusion of unreacted molecules to and into cells as well as on enzymatic conversion to the membrane-impermeable form, which prevents further diffusion. Since CellTracker molecules are commonly used and easy to track, we built a model in which the base case reflected the geometry of a single device pillar (Fig. 2) with estimated diffusive properties and reaction kinetics for CellTracker molecules.[51–56] This parameter set gave a predicted spot size of 374 μm (Fig. 3A–D, represented with a striped bar in Fig. 3B), which was nearest that measured for a 70% confluent cell layer in our experimental dataset, in which the average spot size was 359.2 ± 5.3 μm (a relative difference of 3.7%).

We then investigated how varying separation distances, pillar sizes, diffusion rates, and enzymatic conversion rates might affect patterning. For conditions with modified pillar geometries, our model predicted that patterning from finer features positioned with closer proximity resulted in smaller patterned spot diameters (Fig. 3B). For example, halving the gap from 100 μm to 50 μm and reducing the pillar diameter from 200 μm to 20 μm resulted in a ~102 μm diameter spot size. Thus, fabricating devices with finer features using other fabrication methods (*e.g.*, advanced micro-milling, stereolithography, or precision 3D printing) might further improve patterning resolution by localized diffusive transfer.

To investigate how reaction and diffusion rates might also affect patterning, we identified diffusion rates representative of a small molecule (4.0×10^{-10} m^2 s^{-1}),[57–59] a globular protein (6.4×10^{-11} m^2 s^{-1}),[56,58,60] and a larger protein (properties similar to an antibody, 4.4×10^{-11} m^2 s^{-1})[56,58,61,62] and also selected a range of reaction kinetics corresponding to different potential concentrations of enzyme or catalytic rates. We found that spot size was affected by both diffusion and reaction rate parameters, with more sensitivity to reaction rate for quickly diffusing small molecules (Fig. 3C). Though not representative of a bioactive compound, we established the upper limits of spot size by removing the interaction with the cells entirely. In this case spot size was again most affected (as compared to spot size with cell uptake Fig. 3C) for rapidly diffusing small molecules (Table S1†).

Lastly, we examined model predictions for patterning dynamics. When we tracked spot diameter over time we found little time dependence beyond 30 seconds for a 100 μm gap (Fig. 3D), whereas a 200 μm pillar-to-cell gap showed increased time-dependence (plateauing at 3 min, Fig. 3D). According to the model, depletion of the solute from the device is rapid, with 99% depletion occurring in 30 s to 2 min, depending on diffusion rates (Fig. 3E). Taken together, our experimental and modeling results demonstrate that hydrogel-coated features enable patterned exposure to biomolecules *via* short-term (seconds to minutes) release from patterned features (Fig. 2 and 3A–E) with model predicted dependence on diffusion and reaction properties and device geometry.

Modeling sustained pattern delivery from hydrogel reservoirs

Many biological processes require sequential exposures to biomolecules, or longer incubations to elicit downstream effects. We hypothesized that molding larger hydrogel reservoirs within the devices would facilitate spatial, dynamic, and sustained delivery of solute to cells through diffusion out of reservoirs (Fig. 1B). To test this hypothesis, we used a similar FEM-based approach to determine whether larger reservoirs could indeed maintain more sustained patterning. We

modeled a 24-well plate insert featuring concentric circle reservoirs (Fig. 1B and 3F) and varied the reservoir height parameter (Fig. 3G) to investigate how changes in reservoir volumes might alter dosing of a small molecule across cells over time. We found that the dose taken up by the cell layer over 24 h was greater for reduced reservoir heights under the pattern source (Fig. 3G, point 1) as well as under the neighboring intermediate ring reservoir (Fig. 3G, point 2). Importantly, the relative dose at point 2 as compared to point 1 in Fig. 3G was 16% for a 1 mm reservoir height and 8% for 4 mm-tall reservoirs, indicating improved pattern fidelity for reservoirs with greater heights.

We next more broadly determined how molecule diffusivity (small molecule, protein, and large macromolecule as above) and hinderance stemming from gel pore size (or percent agarose) might affect pattern fidelity. Results indicated that in our parameter space, diffusivity impacted patterning precision (consumption at point 2 relative to point 1 as designated in Fig. 3G) most strongly. Specifically, macromolecules (6.4×10^{-11} m^2 s^{-1} and 4.4×10^{-11} m^2 s^{-1}) showed relatively little unwanted uptake at point 2 in all scenarios over 24 h, whereas small molecule (4.0×10^{-10} m^2 s^{-1}) patterning was more widely dependent on the parameter space (1–3% *vs.* 8–17% consumption at point 2 relative to point 1 for macromolecules *vs.* small molecules, respectively). Finally, we tracked consumption over a 24 h exposure and found that shorter reservoirs gave dosing that plateaued over time while a 4 mm reservoir gave more constant, sustained dosing (Fig. 3I). These considerations led us to fabricate devices with large reservoir volumes for sustained delivery of biological molecules.

Sequential and sustained solute patterning from hydrogel reservoirs

We next experimentally investigated the potential for molded hydrogel (agarose) sources placed in close proximity to cells to serve as reservoirs for solute release. To do this, we first used small molecule CellTracker dyes sourced from gel reservoirs to investigate whether distinct pattern geometries could be patterned sequentially using devices with different features. Using three stamps with two different designs (Fig. 4A and B) we created a complex pattern of regions with separate and overlapping exposures to three cell tracking dyes (Fig. 4C). We exposed HUVECs in 24-well plate format to 1) a concentric ring device containing CellTracker green in the outer ring and center circle (Fig. 4D left), followed by 2) a concentric ring device containing CellTracker red in the intermediate ring (Fig. 4D center, represented as purple), and 3) a "W" device containing CellTracker blue in the "W" gel region (Fig. 4D right). Traces across a cross section of the pattern corresponded to the designed pattern (dark gray lines) for all three dye patterns (Fig. 3E), demonstrating spatial and dynamic control of soluble stimuli to cells in culture using interchangeable device inserts.

In addition to signal sequence, the duration of biological stimuli critically determines how signals are transduced and how cells respond.[63–65] Indeed, many molecules require longer incubations than 5–15 minutes to elicit downstream effects. For example, Tamoxifen-inducible Cre–loxP recombination is widely used to assess phenotypic responses to experimentally controlled changes in gene expression.[66] This genetic modulation requires sustained Tamoxifen exposure and subsequent culture time to induce efficient Cre-mediated loxP excision. We therefore next tested whether our method could be used for sustained patterning to spatially control Tamoxifen-induced gene recombination in cells *in vitro*. We patterned Tamoxifen (372 g mol^{-1}) across primary mouse cardiac fibroblasts that undergo a change from membrane-bound tdTomato expression to GFP expression upon Cre–loxP recombination (Fig. 5A).[67,68] We used device inserts in which Tamoxifen was sourced from a central reservoir of agarose gel (Fig. 5B) to enable sustained delivery and to stabilize the

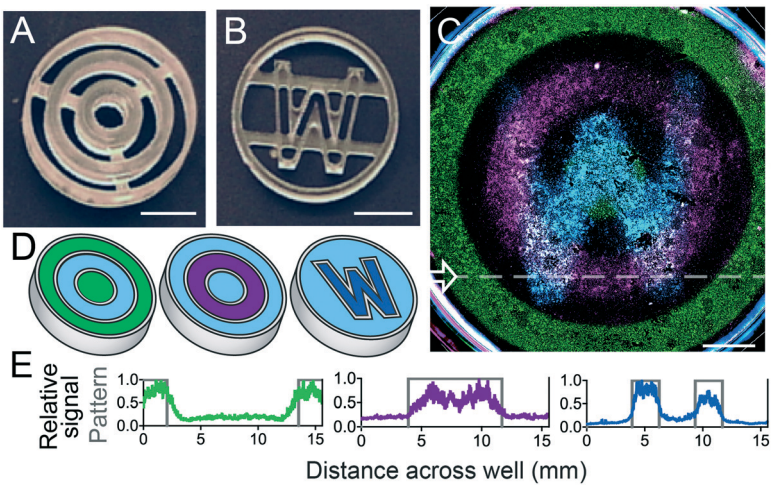

Fig. 4 Sequential pattern application from agarose reservoirs. (A) Concentric ring and (B) "W" devices were used to (C) pattern three cell tracking compounds across well of HUVECs by (D) sequential application in three distinct patterns. (E) Fluorescence signal traces across the well (dashed line in Fig. 3C) were in agreement with the designed pattern. Scale bars: (A and B) 5 mm; (C) 2 mm.

pattern against flow. Following insertion of the device, 12-hour Tamoxifen exposure, and an additional 24 h of culture, recombination was localized to the well center (Fig. 5C and D), as compared to controls in which cells were treated with Tamoxifen in the bulk media (Fig. 5D). To our knowledge, this is the first report to spatially and temporally control widely used forms of Cre–loxP recombination machinery to produce patterned heterogeneity *in vitro*.

The ability of this technique to spatially and dynamically control soluble signals in cell culture using device inserts could open various new avenues of biological research. For example, this ability could be used to probe the mechanisms underlying integration of spatial and temporal information in developmental and regenerative processes,[2,6,8] such as how cells interpret morphogen gradients that emanate across embryos to drive early fate decisions.[3,69] Further, the ability to pattern genetic modulators (*e.g.*, Tamoxifen) could open new avenues of study. For example, local induction of cancer oncogenes could be used to study interactions between malignant foci and surrounding nonmalignant parenchyma and stroma.[70–72]

Spatial localization of viral infection

To further demonstrate the versatility of this method, we next sought to pattern larger diffusing species. We chose to assess the feasibility of patterning viral particles (>100 nm diameter), because viral infection is typically initiated positionally at a specific, localized inoculum from which it then disseminates (as opposed to bulk deposition of particles).[73] Thus, how positional molecular and cellular interactions influence infection from a localized inoculum and spread across a cell population is of interest to infectious disease communities.[73,74]

Our technique relies on diffusion of biomolecule solutes from the device to cells, generally with higher fidelity patterning predicted for decreased rates of diffusion (Fig. 3H). However, for much larger particles applied to the hydrogel in the central reservoir of concentric circle devices (Fig. 6A), impedance to diffusion through the porous network of the gel would preclude efficient loading and release from the bulk of the device. While small molecule diffusion through our agarose matrices could be achieved over several hours, we expected diffusion of viral particles, with diameters approaching the pore size of the agarose gel (~300 nm (ref. 75)), would require prohibitively high doses of virus and long diffusion times. To address this issue, we modified device loading, such that the center chamber of the concentric circle device was loaded with agarose gel and the device was inverted before adding agarose to the outer rings (see methods). The method maintained discontinuity between the three gel compartments and exposed the bottom, cell-facing surface of the center chamber for virus loading. Thereby a small volume of viral particle solution could be placed over and diffuse into the cell-facing surface of only the patterning (center) hydrogel.

Using our modified loading procedure, we first patterned VSV-G pseudotyped lentiviral vector (size ~100 nm, enveloped spherical virion structure) containing a luciferase transgene driven by an albumin promoter across primary rat hepatocytes (Fig. 6B). Quantification of luminescence following the addition of luciferin substrate showed patterned signal in agreement with the templated pattern and significantly modified compared to the uniform control ($p < 0.0001$). We subsequently showed similar patternability for adenovirus (size ~100 nm, naked icosahedral virion structure, Fig. 6C) and Zika virus (size 40 nm, enveloped spherical virion structure, Fig. 6D) when patterned across human embryonic kidney cells 293T (HEK293T), or Vero cells (kidney epithelial cells derived from an African green monkey), respectively. Although virus particles diffused out of the gel and onto the cells over 6–24 hours (depending on the combination of virus and cell type), for all viruses, reporter expression or immunostaining for markers of infection was localized to the centermost subpopulation after device removal and additional culture for 16–48 hours (also host–virus combination dependent, Fig. 6B–E).

These results demonstrate that this method can be used to pattern commonly-used adenovirus and lentivirus vectors

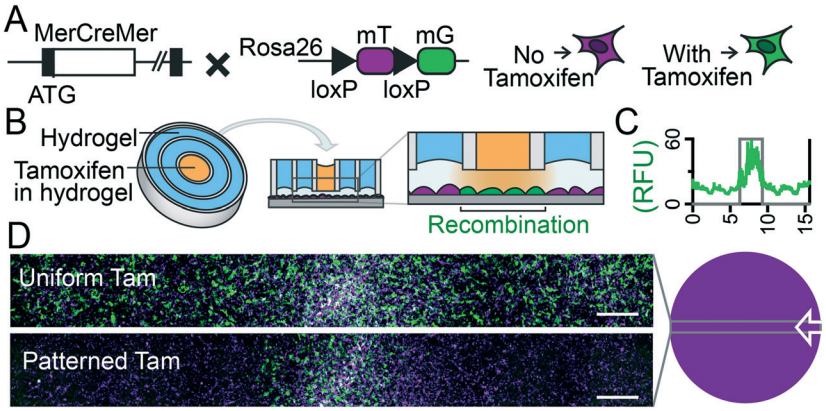

Fig. 5 Sustained release for patterning genetic recombination by Cre–loxP machinery. (A) Cells containing the genetic components for Cre–loxP recombination in primary mouse cardiac fibroblast cultures driving a change in fluorescent reporter expression (purple – tdTomato, to green – GFP) were exposed to a (B) pattern of Tamoxifen sourced from the central well of a concentric ring device. Exposure to the Tamoxifen pattern over 12 h resulted in (C and D) a corresponding pattern in recombination as indicated by expression of GFP. Scale bars: (D) 1 mm.

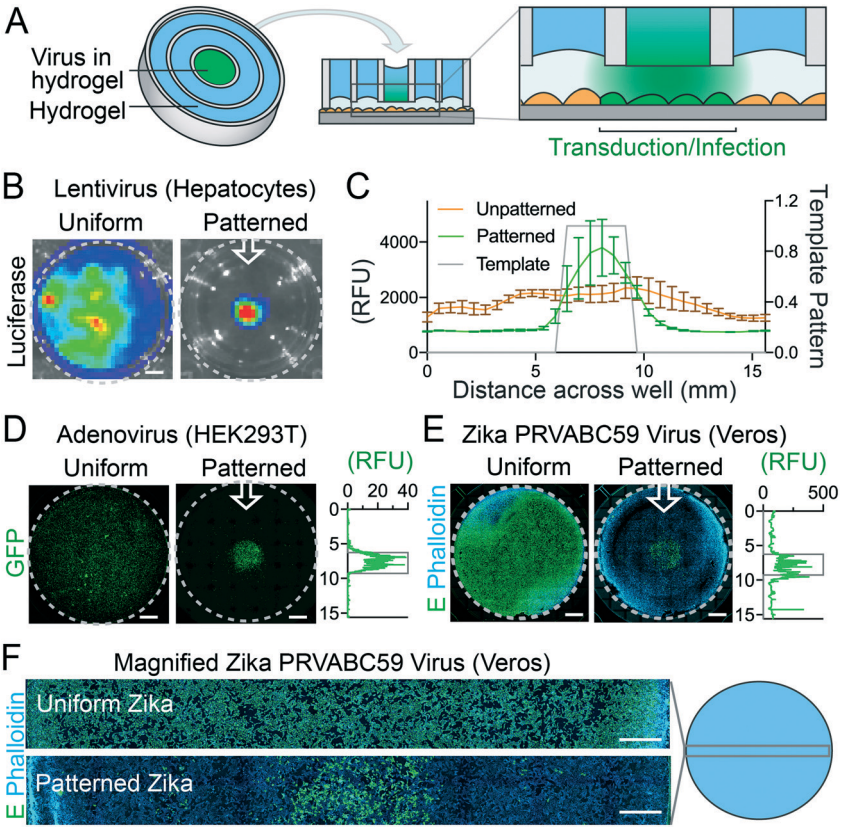

Fig. 6 Viral transduction and infection patterning. (A) Concentric ring devices were used to spatially transfer (B) lentivirus particles to primary rat hepatocytes (luciferase, bioluminescent flux by IVIS), (C) average luminescence signal profiles across wells exposed to patterned and unpatterned lentivirus as in (B). (D) Adenovirus particles to HEK293T cells (green, GFP), and (E and F) Zika virus particles to Vero cell cultures (green, Flavivirus E protein; cyan, phalloidin). Scale bars: (B, D and E) 2 mm; (F) 1 mm.

to regionally deliver genetic material of interest to both primary and immortalized cell types. In future studies, these capabilities may enable users to spatially define heterogeneity in cell phenotype and function as dictated by the viral transgene. Additionally, these data demonstrate patterned inoculation with replication competent and pathogenic Zika virus, which could be used to interrogate spatial host–pathogen relationships such as viral spread and focal propagation of host type 1 interferon response antagonism.[76,77] Such systems may help determine how Zika virus or other pathogens (*e.g.*, Hepatitis C virus or Hepatitis B virus) interfere with host signaling to facilitate their propagation through the local environment.

Conclusions

We present a method for precisely spatially transferring biomolecules to cells *in vitro*. This simple technique solves several critical challenges associated with spatial patterning of biomolecules due to its adaptability in design and application and its robust patterning fidelity. We further demonstrated that this adaptable approach can be used to pattern a variety of biological mediators, including cell tracking compounds, regulators for exogenous cell state control, and pathogenic and gene delivery vectors. This technology offers diverse researchers with a promising entry point to probe and control patterned soluble signals that drive human biology.

Experimental

Device fabrication

To construct device inserts for soluble factor patterning, polystyrene devices were designed in SolidWorks v24 (Dassault Systèmes). SolidWorks parts were converted to G-code using SprutCAM 11 software (SPRUT Technology, Ltd.). Gel-housing and pillar-based patterning devices were milled in 2 mm- or 4 mm-thick polystyrene sheets (Goodfellow USA) using a Tormach PCNC 770 mill (Tormach Inc.) as previously described.[78] Any residual plastic in milled through holes was removed by rinsing or with forceps. For cleaning, devices were rinsed in diH_2O and soaked overnight in 70% ethanol to remove residual mill coolant. Devices were rinsed again in diH_2O and 70% ethanol. In a biosafety cabinet, devices were air-dried and exposed to UV light for at least 20 min, inverted and again exposed to UV light for at least 20 min.

Topographic feature-based label patterning

Human umbilical vein endothelial cells (HUVECs) were seeded at 300 000 cells per well (24-well plate format) 24–48 hours prior to patterning to produce highly confluent

monolayers. Immediately before patterning cells were counterstained with CellTracker Green (10 μM, ThermoFisher) and Hoechst 33342 (10 μg mL^{-1}, ThermoFisher) for 15 min at room temperature (RT), rinsed with media and returned to a 5% CO_2, 37 °C incubator for 20 min. Pillar devices were dipped in 0.5% agarose solution (in PBS) and immediately centrifuged to remove excess agarose. Well bottoms in a 12-well plate were coated with 10× CellTracker Red (100 μM, ThermoFisher). Each pillar array was placed into a CellTracker-containing well so that the outer ring and pillar tips contacted the dye layer. CellTracker dye was absorbed for 5 min at RT. The device was then removed, immersed twice in sterile PBS (Gibco), and placed in a HUVEC-seeded well completely filled with media (pillars facing down). Excess media was aspirated, lowering the device until its outer ring contacted the cell culture surface, but with a continuous layer of media remaining between the device and the culture surface. Media was aspirated through a central venting port of the device allowing rapid, uniform lowering until the outer offset ring contacted the cell surface. Due to the high fluidic resistance within the agarose hydrogel, the gel that contains the patterned solute retains and stabilizes the pattern during device lowering despite fluid flow from below the device. This process Following a 5 min incubation at RT for pattern transfer, media was added causing the device to float up from the culture surface for removal. Cells were rinsed twice in media and live imaged using a Nikon Ti-E inverted microscope (Nikon Instruments, Melville NY) equipped with a CoolSNAP HQ2 monochrome camera (Photometrics, Tucson, AZ) run with the Nikon NIS Elements Software version 4.51 within 2 h of patterning.

Patterning from agarose hydrogels

24 h before sequential agarose gel-sourced dye patterning, HUVECs were seeded at 300 000 cells per well (24-well plate format) to produce confluent monolayers. 4 h before dye transfer to cells all rings in concentric circle devices and the spaces within and surrounding a 'W' design device were filled 2/3-full with 3% agarose (SeaPlaque; Lonza) in PBS. For each well one concentric ring device received 10× CellTracker green in the outer ring and central region, one concentric ring device received 10× CellTracker red in the middle ring, and one 'W' device received 10× CellTracker blue within the 'W' region. At the time of placement, the overlying CellTracker solution was removed from the device containing CellTracker green, the device was rinsed in HUVEC media, and placed above wells completely filled with media. Excess media was aspirated to lower the device to the cell culture surface positioning the lower surfaces of the gels and internal device features approximately 100 μm above the culture surface. Media was aspirated from around the edge of the device through a 200 μL pipette tip allowing gradual, uniform lowering without device tipping until the outer offset feet contacted the cell surface. To initiate aspiration slight pressure was applied to the top of the device with the pipette tip such that device entered the well completely and media rose around the device. Due to the high fluidic resistance within the agarose hydrogel, the gel that contained the patterned solute retained and stabilized the pattern during device lowering despite fluid flow from below the device. After a 15 min incubation at RT media was added to float devices for removal and cell layers were rinsed twice in media and returned to a 5% CO_2, 37 °C incubator 10 min. Device preparation, placement, incubation, and removal was repeated with the devices containing CellTrackers red and blue. Following a final 10 min incubation in a 5% CO_2, 37 °C incubator, wells were imaged using a Nikon Ti-E inverted microscope.

For patterned genetic recombination, the day before pattern placement, primary mouse fibroblasts were seeded at 120 000 cells per well (24-well format) and media was changed to DMEM with 2% FBS, 1% Pen–Strep to slow proliferation. 3% agarose in PBS was molded in concentric circle devices. For Tamoxifen (Sigma-Aldrich) patterning, all rings in the mold were filled 2/3-full with agarose and the devices were covered in fibroblast media (DMEM with 10% FBS, 1% Pen–Strep) overnight at RT. At the time of treatment central positive and negative control wells were treated with or without 0.5 ng mL^{-1} Tamoxifen in media respectively. Concentric circle devices were placed above wells filled completely with media and media was aspirated as described for devices containing gel reservoirs above until the outer ring of the devices contacted the culture surface positioning the lower surfaces of the gels and internal device features 100 μm above the culture surface. All excess media was removed from above the devices and 3 mg mL^{-1} unpolymerized collagen containing 0.5 ng mL^{-1} Tamoxifen was added above the center agarose gel. Well plates were returned to a 5% CO_2, 37 °C incubator for 12 h. Media was added to float devices for removal and cell layers were rinsed twice in media and returned to DMEM with 2% FBS, 1% Pen–Strep and place in a 5% CO_2, 37 °C incubator for 24 h. Wells were then live imaged for tdTomato and eGFP expression using a Nikon Ti-E inverted microscope.

For virus patterning, 3% agarose was added to the center circle of concentric circle devices, molded against glass coverslips, and allowed to gel. Devices were then inverted and agarose in the outer two rings were molded against a glass coverslips. The devices were incubated in media overnight. Rat hepatocytes (300 000 cells per well), HEK293T (150 000 cells per well), or Vero cells (150 000 cells per well) were seeded in 24-well plates and cultured for 2 days (hepatocytes) or 1 day (HEK293T, Vero). Media was completely removed from the devices 18 h before placement and 5 μL of virus containing solution was added to the cell-facing surface of the center circle. Devices were placed in a humidified and sealed chamber at 4 °C overnight. The following day devices were rinsed 3–5 times in PBS and placed in wells filled with media with the virus-absorbing surface of the center circle facing downwards. Excess media was aspirated as described for devices containing gel reservoirs above to lower the devices to the well culture surfaces and plates were place in a 5% CO_2, 37

°C incubator for 6 h (lentivirus), 24 h (adenovirus), or 8 h (Zika virus). After virus pattern transfer, devices were floated with media and removed, cell layers were rinsed with media, and cultures were returned to a 5% CO_2, 37 °C incubator. Hepatocytes were live imaged by IVIS (IVIS Spectrum *in vivo* Imaging System; PerkinElmer Inc.) after 48 h of culture and within 15 min of adding D-luciferin substrate (150 μg mL^{-1}, Gold Biotechnology). After 24 h of culture HEK293-T wells were live imaged for GFP expression. Vero cultures were fixed after 20 h of culture for subsequent immunostaining.

Finite element modeling

We generated models for the transport of diffusing species using our pillar device (a single pillar in the array) and concentric circle device geometries in COMSOL Multiphysics software (v5.1; COMSOL Inc.). Diffusion parameters for small molecules (similar to CellTrackers), small macromolecules, and large macromolecules were estimated based on the literature[55–60,62,79–81] (Tables S2 and S3†). Transport through cell media was modeled as free-diffusion and hindered diffusion was assumed and estimated depending on gel density and the size of the diffusing species according to established correlations[56–58] (Table S4†). In the model unreacted solute (analogous to CellTracker) was sourced at the pillar tip, reached the cell layer *via* free diffusion, and became nondiffusible in the cell layer according to Michaelis–Menten kinetics (for the base case enzyme concentration of 1 mM).[52,54] Enzymatic conversation kinetics of CellTrackers were modeled using the Michaelis–Menten equation and parameters for the relevant enzyme, glutathione *s*-transferase, based on the literature.[51,52,54] For varied reaction rates the range of the V_{max} constant ([enzyme] × kcat) of the Michaelis–Menten equation spanned five orders of magnitude and expressed as equivalent enzyme concentration (Tables S2 and S4†). Spot diameters were quantified as twice the distance between the spot center and the point at which the concentration of reaction product was reduced by one order of magnitude from the maximum. For our model of a concentric reservoir device, 0.1% or 0.001% per second efficiencies were selected as generalized consumption rates in the cell monolayer. Including consumption allowed us to track relative dosing across the cell layer over time and for different configuration. These two rates were selected as they allowed lateral diffusion between reservoirs similar to a consumption-free configuration (data not shown). These rates therefore represented a lower performance case than scenarios with more rapid consumption, which would improve pattern fidelity. When tracking dosing stability over time we modeled the scenario with most rapid reservoir depletion (small molecule consumed at 0.1%/s). Total source dosing was held constant by normalization for changes in pillar or reservoir geometries.

Cell culture

Human umbilical vein endothelial cells (HUVECs, Lonza) were maintained in EGM-2 media (Lonza) and seeded for patterning at passages 4–8. HEK293T (ATCC) were maintained in DMEM with high glucose (4.5 g L^{-1}) and L-glutamine (Corning), 10% fetal bovine serum (FBS, Biowest USA) and 1% Penicillin–Streptomycin (Pen–Strep, HyClone). HEK293A cells were maintained in DMEM with high glucose and L-glutamine (Corning), 10% bovine calf serum (HyClone) and 1% Pen–Strep (Corning). Rat hepatocytes were isolated from adult female Lewis rats (Envigo) by collagenase perfusion using methods described previously.[82,83] Briefly, animals were anesthetized with isoflurane, the portal vein was cannulated, and the liver was perfused and digested with collagenase type IV (Sigma-Aldrich). Hepatocytes were purified from the digest using Percoll (GE Healthcare) centrifugation and then seeded at a density of 300 000 cells per well per a 24-well plate adsorbed with 0.14 mg ml^{-1} rat tail collagen I (Corning). Primary rat hepatocytes were maintained in DMEM with high glucose and L-glutamine (Corning), 10% FBS (Biowest), 0.04 μg ml^{-1} dexamethasone (Sigma-Aldrich), 7 ng ml^{-1} glucagon (Sigma-Aldrich), 1% ITS+ culture supplement (Corning), 1.5% 1 M HEPES (Gibco), and 1% Pen–Strep (HyClone). Primary mouse cardiac fibroblasts were isolated by Langendorff perfusion as previously described[84] and maintained for two passages in DMEM with high glucose and L-glutamine (HyClone) with 20% FBS (Seradigm) and 1% Pen–Strep (Corning) prior to seeding for experiments. Cardiac fibroblasts inducibly expressed Cre recombinase (Tamoxifen-driven MerCreMer sequence) from the Tcf21 (cardiac fibroblast-specific) locus and contained a Rosa26 mt mg^{-1} reporter construct as previously described.[67] Vero cells (ATCC) were cultured in medium comprised of MEM (ThermoFisher) supplemented with 10% FBS (VWR), 1× non-essential amino acids (ThermoFisher), 50 units per mL of penicillin and 50 μg mL^{-1} of streptomycin (ThermoFisher). The *Aedes albopictus* derived cell line C6/36 (ATCC) was propagated at 28 °C in 5% CO_2 in medium comprised of MEM supplemented with 10% FBS (VWR), 1× non-essential amino acids, 50 units per mL of penicillin and 50 μg mL^{-1} of streptomycin (ThermoFisher). The B lymphocyte hybridoma cell line D1-4G2-4-15 was obtained from ATCC and maintained in ATCC Hybri-Care Medium supplemented with 10% FBS (VWR) and 1.5 g L^{-1} sodium bicarbonate. All cells were maintained in standard cell culture treated polystyrene vessels before seeding for patterning.

Virus production

Lentiviral plasmid encoding firefly luciferase under the human albumin promoter (pTRIP.Alb.Fluc.IRES.tagRFP.NLS-IPS, gift of Charles Rice, The Rockefeller University) was packaged using HEK293T cells and concentrated using ultracentrifugation. Adenovirus constitutively expressing GFP[85,86] was produced in HEK293A cells and collected as crude supernatant cleared of cellular debris by centrifugation. Zika virus strain PRVABC59 (Puerto Rico 2015) was obtained from the ATCC. Virus was propagated by infecting 80% confluent C6/36 monolayers with low-passage stock virus at an MOI of 0.01,

and harvesting infectious supernatants 5–7 days postinfection. Infectious supernatants were cleared of cellular debris by centrifugation. All viruses were stored at −80 °C until use.

Immunohistochemistry

To stain Zika-infected cultures, 20 h after patterning device removal cultures were fixed with 4% PFA in PBS for 15 minutes at RT. Cells were then permeabilized with 0.1% Triton X-100 in PBS for 10 minutes at RT and blocked with 5% normal goat serum in 0.05% Tween-20/PBS. Cells were then stained with Flavivirus E protein (4G2) antibody (2 μg mL^{-1} in blocking buffer) purified from hybridoma supernatants using protein A/G chromatography. Primary antibody incubation was followed by anti-mouse Alexafluor 594 conjugated secondary antibody (ThermoFisher) together with Phalloidin-Alexafluor 488 (ThermoFisher).

Image analysis

Patterning in well plate format was quantified for a 500 μm wide strip bisecting or spanning the full width of the well using the "Plot Profile" function in ImageJ. Representative pattern profiles were then overlayed with the corresponding designed pattern of pillars or the agarose source gel compartment. Pillar-patterned spot centroids were identified by uniformly applying "Erode" and "Dilate" functions in ImageJ to obtain continuous spots in binary images. Centroid coordinates were located using the ImageJ "Analyze particles" function. Centroid plots for the four replicates were aligned to their average spot positions and distances between replicate spots were calculated using the standard distance formula. Spot size was quantified in ImageJ by a blinded observer and cell density was quantified using the "Watershed" and "Analyze particles" functions in ImageJ. Cell counts were normalized to the estimated cell coverage of 80% for the highest density condition.

Statistical analysis

Statistical analysis was performed in GraphPad Prism v7.0c. Error bars denote standard error of the mean and statistical significance between multiple groups was assessed by ordinary one-way ANOVA or two-way ANOVA with Tukey's multiple comparisons post-hoc test. $p < 0.05$ was considered statistically significant.

Conflicts of interest

The authors declare the following competing financial interests: D. J. B. holds equity in Bellbrook Labs LLC, Tasso Inc., Salus Discovery LLC, Stacks to the Future LLC and Onexio Biosystems LLC. E. B. has ownership in Tasso, Inc.; and Stacks to the Future, LLC.

Acknowledgements

We would like to thank Dr. Dale Hailey and the Garvey Cell Imaging Lab for assistance with fluorescence microscopy and Dr. Ashleigh Theberge for providing access to equipment for micromilling. This research was funded by NIH grants DP2HL137188 (K. R. S.), R01GM101183 (A. K.), R21 AI124266 (J. D. A.), P41 GM109824 (J. D. A.), and P30CA014520 (D. J. B.). M. C. R. was supported by NIH Grant T32GM008349 and a WRF postdoctoral fellowship. E. O. was supported by NIH/NIBIB T32EB001650.

References

1 K. M. Loh, R. van Amerongen and R. Nusse, *Dev. Cell*, 2016, **38**, 643–655.
2 A. D. Lander, *Science*, 2013, **339**, 923–927.
3 E. Bier and E. M. De Robertis, *Science*, 2015, **348**, aaa5838.
4 K. W. Rogers and A. F. Schier, *Annu. Rev. Cell Dev. Biol.*, 2011, **27**, 377–407.
5 P. Friedl and D. Gilmour, *Nat. Rev. Mol. Cell Biol.*, 2009, **10**, 445–457.
6 B.-S. Ding, D. J. Nolan, J. M. Butler, D. James, A. O. Babazadeh, Z. Rosenwaks, V. Mittal, H. Kobayashi, K. Shido, D. Lyden, T. N. Sato, S. Y. Rabbany and S. Rafii, *Nature*, 2010, **468**, 310–315.
7 D. Hanahan and R. A. Weinberg, *Cell*, 2011, **144**, 646–674.
8 S. de Oliveira, E. E. Rosowski and A. Huttenlocher, *Nat. Rev. Immunol.*, 2016, **16**, 378–391.
9 S. M. Lindsay and J. Yin, *AIChE J.*, 2016, **62**, 2227–2233.
10 J. Atencia and D. J. Beebe, *Nature*, 2005, **437**, 648–655.
11 Y. Tabata and M. P. Lutolf, *Sci. Rep.*, 2017, **7**, 44711.
12 C. G. Sip, N. Bhattacharjee and A. Folch, *Lab Chip*, 2014, **14**, 302–314.
13 T. M. Keenan and A. Folch, *Lab Chip*, 2008, **8**, 34–57.
14 J. Atencia, J. Morrow and L. E. Locascio, *Lab Chip*, 2009, **9**, 2707.
15 N. Li Jeon, H. Baskaran, S. K. W. Dertinger, G. M. Whitesides, L. Van de Water and M. Toner, *Nat. Biotechnol.*, 2002, **20**, 826–830.
16 D. Irimia, D. A. Geba and M. Toner, *Anal. Chem.*, 2006, **78**, 3472–3477.
17 S. Tay, J. J. Hughey, T. K. Lee, T. Lipniacki, S. R. Quake and M. W. Covert, *Nature*, 2010, **466**, 267–271.
18 V. V. Abhyankar, M. A. Lokuta, A. Huttenlocher and D. J. Beebe, *Lab Chip*, 2006, **6**, 389.
19 T. M. Keenan, C.-H. Hsu and A. Folch, *Appl. Phys. Lett.*, 2006, **89**, 114103.
20 B. G. Chung, F. Lin and N. L. Jeon, *Lab Chip*, 2006, **6**, 764–768.
21 D. Juncker, H. Schmid and E. Delamarche, *Nat. Mater.*, 2005, **4**, 622–628.
22 M. A. Qasaimeh, T. Gervais and D. Juncker, *Nat. Commun.*, 2011, **2**, 464.
23 D. Chen, W. Du, Y. Liu, W. Liu, A. Kuznetsov, F. E. Mendez, L. H. Philipson and R. F. Ismagilov, *Proc. Natl. Acad. Sci. U. S. A.*, 2008, **105**, 16843–16848.

24 G. V. Kaigala, R. D. Lovchik, U. Drechsler and E. Delamarche, *Langmuir*, 2011, **27**, 5686–5693.
25 H. Tavana, A. Jovic, B. Mosadegh, Q. Y. Lee, X. Liu, K. E. Luker, G. D. Luker, S. J. Weiss and S. Takayama, *Nat. Mater.*, 2009, **8**, 736–741.
26 D. Irimia, S.-Y. Liu, W. G. Tharp, A. Samadani, M. Toner and M. C. Poznansky, *Lab Chip*, 2006, **6**, 191–198.
27 C. M. Perrault, M. A. Qasaimeh, T. Brastaviceanu, K. Anderson, Y. Kabakibo and D. Juncker, *Rev. Sci. Instrum.*, 2010, **81**, 115107.
28 S. Elizabeth Hulme, S. S. Shevkoplyas and G. M. Whitesides, *Lab Chip*, 2009, **9**, 79–86.
29 M. A. Unger, *Science*, 2000, **288**, 113–116.
30 Kshitiz, D.-H. Kim, D. J. Beebe and A. Levchenko, *Trends Biotechnol.*, 2011, **29**, 399–408.
31 E. Berthier, E. W. K. Young and D. Beebe, *Lab Chip*, 2012, **12**, 1224.
32 A. M. Shah, M. Yu, Z. Nakamura, J. Ciciliano, M. Ulman, K. Kotz, S. L. Stott, S. Maheswaran, D. A. Haber and M. Toner, *Anal. Chem.*, 2012, **84**, 3682–3688.
33 E. K. Sackmann, A. L. Fulton and D. J. Beebe, *Nature*, 2014, **507**, 181–189.
34 G. M. Walker, J. Sai, A. Richmond, M. Stremler, C. Y. Chung and J. P. Wikswo, *Lab Chip*, 2005, **5**, 611.
35 L. Masaro and X. X. Zhu, *Prog. Polym. Sci.*, 1999, **24**, 731–775.
36 E. Y. Tokuda, J. L. Leight and K. S. Anseth, *Biomaterials*, 2014, **35**, 4310–4318.
37 T. Yeung, P. C. Georges, L. A. Flanagan, B. Marg, M. Ortiz, M. Funaki, N. Zahir, W. Ming, V. Weaver and P. A. Janmey, *Cell Motil. Cytoskeleton*, 2005, **60**, 24–34.
38 D. Hanjaya-Putra, J. Yee, D. Ceci, R. Truitt, D. Yee and S. Gerecht, *J. Cell. Mol. Med.*, 2010, **14**, 2436–2447.
39 W. Yu, H. Qu, G. Hu, Q. Zhang, K. Song, H. Guan, T. Liu and J. Qin, *PLoS One*, 2014, **9**, e89966.
40 U. Liegibel, U. Sommer, B. Bundschuh, B. Schweizer, U. Hilscher, A. Lieder, P. Nawroth and C. Kasperk, *Exp. Clin. Endocrinol. Diabetes*, 2004, **112**, 356–363.
41 S. Boyden, *J. Exp. Med.*, 1962, **115**, 453–466.
42 S. B. Berry, T. Zhang, J. H. Day, X. Su, I. Z. Wilson, E. Berthier and A. B. Theberge, *Lab Chip*, 2017, **17**, 4253–4264.
43 S. C. Oppegard, A. J. Blake, J. C. Williams and D. T. Eddington, *Lab Chip*, 2010, **10**, 2366.
44 S. Cosson and M. P. Lutolf, *Sci. Rep.*, 2014, **4**, 4462.
45 D. J. Beebe, G. A. Mensing and G. M. Walker, *Annu. Rev. Biomed. Eng.*, 2002, **4**, 261–286.
46 T. M. Squires and S. R. Quake, *Rev. Mod. Phys.*, 2005, **77**, 977–1026.
47 N. Crosetto, M. Bienko and A. van Oudenaarden, *Nat. Rev. Genet.*, 2015, **16**, 57–66.
48 K. B. Halpern, R. Shenhav, O. Matcovitch-Natan, B. Tóth, D. Lemze, M. Golan, E. E. Massasa, S. Baydatch, S. Landen, A. E. Moor, A. Brandis, A. Giladi, A. Stokar-Avihail, E. David, I. Amit and S. Itzkovitz, *Nature*, 2017, **542**, 352–356.
49 S. Pandey, K. Shekhar, A. Regev and A. F. Schier, *Curr. Biol.*, 2018, **28**, 1052–1065, e7.
50 B. S. Katzenellenbogen, M. M. Montano, K. Ekena, M. E. Herman and E. M. McInerney, *Breast Cancer Res. Treat.*, 1997, **44**, 23–38.
51 A. K. Godwin, A. Meister, P. J. O'Dwyer, C. S. Huang, T. C. Hamilton and M. E. Anderson, *Proc. Natl. Acad. Sci. U. S. A.*, 1992, **89**, 3070–3074.
52 M. Moron, J. Depierre and B. Mannervik, *Biochim. Biophys. Acta, Gen. Subj.*, 1979, **582**, 67–78.
53 I. de Waziers, P. H. Cugnenc, C. S. Yang, J. P. Leroux and P. H. Beaune, *J. Pharmacol. Exp. Ther.*, 1990, **253**, 387–394.
54 T. A. Enache and A. M. Oliveira-Brett, *Bioelectrochemistry*, 2015, **101**, 46–51.
55 N. Periasamy and A. S. Verkman, *Biophys. J.*, 1998, **75**, 557–567.
56 E. M. Johnson, D. A. Berk, R. K. Jain and W. M. Deen, *Biophys. J.*, 1996, **70**, 1017–1023.
57 D. S. Clague and R. J. Phillips, *Phys. Fluids*, 1996, **8**, 1720–1731.
58 N. Fatin-Rouge, K. Starchev and J. Buffle, *Biophys. J.*, 2004, **86**, 2710–2719.
59 C. B. Müller, A. Loman, V. Pacheco, F. Koberling, D. Willbold, W. Richtering and J. Enderlein, *EPL*, 2008, **83**, 46001.
60 A. Pluen, P. A. Netti, R. K. Jain and D. A. Berk, *Biophys. J.*, 1999, **77**, 542–552.
61 A. Hawe, W. L. Hulse, W. Jiskoot and R. T. Forbes, *Pharm. Res.*, 2011, **28**, 2302–2310.
62 W. M. Saltzman, M. L. Radomsky, K. J. Whaley and R. A. Cone, *Biophys. J.*, 1994, **66**, 508–515.
63 N. Miskov-Zivanov, M. S. Turner, L. P. Kane, P. A. Morel and J. R. Faeder, *Sci. Signaling*, 2013, **6**, ra97.
64 F. Etoc, J. Metzger, A. Ruzo, C. Kirst, A. Yoney, M. Z. Ozair, A. H. Brivanlou and E. D. Siggia, *Dev. Cell*, 2016, **39**, 302–315.
65 M. Tewary, J. Ostblom, L. Prochazka, T. Zulueta-Coarasa, N. Shakiba, R. Fernandez-Gonzalez and P. W. Zandstra, *Development*, 2017, **144**, 4298–4312.
66 S. Hayashi and A. P. McMahon, *Dev. Biol.*, 2002, **244**, 305–318.
67 A. Acharya, S. T. Baek, S. Banfi, B. Eskiocak and M. D. Tallquist, *Genesis*, 2011, **49**, 870–877.
68 O. Kanisicak, H. Khalil, M. J. Ivey, J. Karch, B. D. Maliken, R. N. Correll, M. J. Brody, S.-C. J. Lin, B. J. Aronow, M. D. Tallquist and J. D. Molkentin, *Nat. Commun.*, 2016, **7**, 12260.
69 D. Ben-Zvi, B.-Z. Shilo, A. Fainsod and N. Barkai, *Nature*, 2008, **453**, 1205–1211.
70 S. P. Leong, A. Aktipis and C. Maley, *Clin. Exp. Metastasis*, 2018, **35**, 361.
71 M. M. Merino, R. Levayer and E. Moreno, *Trends Cell Biol.*, 2016, **26**, 776–788.
72 F. Guo, Y. Wang, J. Liu, S. C. Mok, F. Xue and W. Zhang, *Oncogene*, 2016, **35**, 816–826.
73 F. Akpinar, B. Inankur and J. Yin, *J. Virol.*, 2016, **90**, 7552–7566.
74 J. Muffat, Y. Li, A. Omer, A. Durbin, I. Bosch, G. Bakiasi, E. Richards, A. Meyer, L. Gehrke and R. Jaenisch, *Proc. Natl. Acad. Sci. U. S. A.*, 2018, **115**, 7117–7122.

75 N. Pernodet, M. Maaloum and B. Tinland, *Electrophoresis*, 1997, **18**, 55–58.
76 J. R. Bowen, K. M. Quicke, M. S. Maddur, J. T. O'Neal, C. E. McDonald, N. B. Fedorova, V. Puri, R. S. Shabman, B. Pulendran and M. S. Suthar, *PLoS Pathog.*, 2017, **13**, e1006164.
77 A. Grant, S. S. Ponia, S. Tripathi, V. Balasubramaniam, L. Miorin, M. Sourisseau, M. C. Schwarz, M. P. Sánchez-Seco, M. J. Evans, S. M. Best and A. García-Sastre, *Cell Host Microbe*, 2016, **19**, 882–890.
78 D. J. Guckenberger, T. E. de Groot, A. M. D. Wan, D. J. Beebe and E. W. K. Young, *Lab Chip*, 2015, **15**, 2364–2378.
79 J. K. Armstrong, R. B. Wenby, H. J. Meiselman and T. C. Fisher, *Biophys. J.*, 2004, **87**, 4259–4270.
80 T. C. Laurent, L.-O. Sundelof, K. O. Wik and B. Warmegard, *Eur. J. Biochem.*, 1976, **68**, 95–102.
81 L.-Z. He and B. Niemeyer, *Biotechnol. Prog.*, 2003, **19**, 544–548.
82 P. O. Seglen, in *Methods in Cell Biology*, Elsevier, 1976, vol. 13, pp. 29–83.
83 K. R. Stevens, M. D. Ungrin, R. E. Schwartz, S. Ng, B. Carvalho, K. S. Christine, R. R. Chaturvedi, C. Y. Li, P. W. Zandstra, C. S. Chen and S. N. Bhatia, *Nat. Commun.*, 2013, **4**, 1847.
84 J. D. Molkentin, D. Bugg, N. Ghearing, L. E. Dorn, P. Kim, M. A. Sargent, J. Gunaje, K. Otsu and J. Davis, *Circulation*, 2017, **136**, 549–561.
85 J. Davis, A. R. Burr, G. F. Davis, L. Birnbaumer and J. D. Molkentin, *Dev. Cell*, 2012, **23**, 705–715.
86 J. Xu, N. L. Gong, I. Bodi, B. J. Aronow, P. H. Backx and J. D. Molkentin, *J. Biol. Chem.*, 2006, **281**, 9152–9162.